PAPER

Visualizing microcalcifications in lumpectomy specimens: an exploration into the clinical potential of carbon nanotube-enabled *stationary* digital breast tomosynthesis

RECEIVED
3 May 2019

REVISED
1 July 2019

ACCEPTED FOR PUBLICATION
17 July 2019

PUBLISHED
25 July 2019

Connor Puett[1], **Jenny Gao**[1], **Andrew Tucker**[1], **Christina R Inscoe**[2], **Michael Hwang**[3], **Cherie M Kuzmiak**[3], **Jianping Lu**[2], **Otto Zhou**[2] and **Yueh Z Lee**[1,2,3]

[1] UNC/NCSU Joint Department of Biomedical Engineering, The University of North Carolina at Chapel Hill, Chapel Hill, NC, 27599, United States of America
[2] Department of Physics and Astronomy, The University of North Carolina at Chapel Hill, Chapel Hill, NC 27599, United States of America
[3] Department of Radiology, The University of North Carolina at Chapel Hill, Chapel Hill, NC, 27599, United States of America

E-mail: connor_puett@med.unc.edu

Keywords: *stationary* digital breast tomosynthesis, DBT, 3D mammography, microcalcifications, breast specimens, magnified mammography

Abstract

Purpose: To assess the visibility of microcalcifications in images generated by a first-generation carbon-nanotube (CNT)-enabled *stationary* digital breast tomosynthesis (sDBT) device, using magnified 2D mammography and conventional, moving-source DBT as references for comparison. *Methods*: Lumpectomy specimens were imaged by magnified mammography and two 3D mammography approaches, including sDBT and moving-source DBT. The planar size of individual microcalcifications was measured in the reconstructed image stacks of sDBT and moving-source DBT and compared to the magnified mammography image. An artifact spread function (ASF) was used to assess the depth dimensions of the microcalcifications displayed through the reconstructed image stacks. Breast-imaging specialists rated their preference for one imaging modality over another when interpreting microcalcifications in the magnified mammography image and synthetic slab images from sDBT and moving-source DBT. *Results*: The planar size of individual microcalcifications was similar in images generated by sDBT and moving-source DBT when the sDBT projections were binned to match the pixel size used by the moving-source DBT system. However, the unique structure of sDBT allowed for a wider-angle span of projection views and operation of the detector in full-resolution mode without significantly compromising the scan time. In this configuration, the planar sizes of individual microcalcifications displayed by sDBT was more similar to magnified mammography than moving-source DBT, and the microcalcifications had a narrower ASF through depth. Readers preferred sDBT over moving-source DBT when assessing microcalcifications in synthetic slab images, although magnified mammography was rated highest overall. *Conclusions*: The sDBT system displayed microcalcifications as well as conventional, moving-source DBT when the effective pixel size of the detector was matched. However, with the detector in its full-resolution mode, sDBT displayed microcalcifications with greater clarity. Readers still preferred images generated by magnified mammography over both 3D mammography approaches. This finding is guiding continued hardware and software development to optimize the sDBT technology.

1. Introduction

Breast cancer is by far the most common non-skin malignancy in women, responsible for more cases than the next two common cancer types (lung and colorectal) combined [1]. In 2018, more than 250,000 Americans were diagnosed with breast cancer, and at least 40,000 died from it [1]. Since survival correlates strongly with the extent of disease at the time of discovery, screening is used to identify cancer at an early or localized stage. The American College of Radiology recommends annual mammography

screening for all women with an average risk of developing breast cancer beginning at age 40 [2]. However, since standard mammograms collapse the three-dimensional (3D) breast anatomy into a single 2D image, concerning features can be obscured and overlapping features can mimic pathology. As a result, the sensitivity of mammography for breast cancer detection averages less than 90%, and call-backs for false positive findings are common [3–5].

Delivering a radiation dose similar to mammography, digital breast tomosynthesis (DBT) may turn out to be a more effective screening tool than standard mammography [6, 7]. Now recognized as 3D mammography, DBT was approved for clinical use by the Food and Drug Administration (FDA) in 2011, following studies demonstrating an improved detection of breast masses as well as a decrease in the number of call-back diagnostic studies for false positive findings when used with mammography, compared to standard screening mammography alone [8–12]. DBT is a limited-angle tomography. The examination involves collecting a series of oblique projection views across a relatively narrow angular span. The 2D information from these projections is then processed by computer algorithms to reconstruct a 3D image space, which is displayed as a stack of image slices. Only the in-focus features in each slice are present at that anatomic depth, thus decreasing the chance that overlapping features will obscure important findings.

However, the technical steps required to obtain this depth information, as well as the post-acquisition processing needed to display it, introduce unique problems that affect the resolution of the imaging systems and thus the quality of the images presented to the reader. Specifically, concern has been raised over the visibility of microcalcifications [13, 14]. Along with masses, the morphology of individual microcalcifications and the spatial relationship of microcalcification clustering are key diagnostic features in mammography [15]. Hence, DBT is most commonly used in combination with standard 2D mammography [16], effectively doubling the radiation dose and prolonging the uncomfortable time of breast compression. Advances in both technology and image processing are addressing the challenges with DBT, with a goal of eliminating the need to get a standard mammogram at the same time. For example, image processing that generates a synthetic mammogram has been approved in several systems [17, 18]. *Stationary* DBT (sDBT) is a novel approach to 3D mammography [19, 20]. It was developed to address the limitations of the currently-available DBT systems imposed by their moving x-ray source.

Commercially-available 3D mammography devices, which will be referred to as moving-source DBT for consistency, must translate a standard x-ray tube through space to collect projection views. In contrast, sDBT uses a fixed array of separate and distributed x-ray sources made possible by carbon nanotube (CNT) cathodes [19, 20]. The purpose of this study was to evaluate the visibility of microcalcifications in images of lumpectomy specimens collected by sDBT, using magnified 2D mammography and the parent moving-source DBT system, from which the sDBT device was constructed, as references for comparison. The findings of this study have important clinical implications, as improving the visibility of microcalcifications may be the key advance by which DBT replaces standard mammography as the breast imaging tool of choice.

2. Materials and methods

2.1. Selecting and handling the breast specimens

Twenty-three women with Breast Imaging and Reporting Data System (BIRADS) 4 or 5 lesions ('suspicious abnormality' or 'highly suspicious for malignancy') were recruited following study approval by the University of North Carolina at Chapel Hill Institutional Review Board (IRB). The concerning breast lesions had been discovered and evaluated by standard screening and diagnostic imaging, and the patients were awaiting lumpectomy following a needle localization procedure. Standard protocol at our institution includes magnified (1.8×) imaging of all lumpectomy specimens using 2D digital mammography in order to define lesion margins. The specimens are gently compressed over a perforated and labelled grid to prevent motion and allow identification of feature location in the x-ray image (figure 1(A)), placed on a magnification stand, and imaged using a substantially smaller x-ray focal spot compared to conventional 2D mammography, thereby providing a higher image resolution. Following this standard imaging step, the contained specimens were also imaged by sDBT and the commercially-available, moving-source DBT device from which the sDBT system was constructed. After imaging, the specimens were transferred to the Department of Pathology.

2.2. Acquiring the projection views

Images were obtained by a Selenia Dimensions 2D and 3D mammography unit (Hologic Inc., Bedford, MA) and by sDBT. The first-generation sDBT device was a modified Selenia Dimensions machine in which the single x-ray source was replaced by a fixed array of CNT-enabled sources (figure 1(B)). Both sDBT and moving-source DBT were operated at 26 kVp, using a total exposure of 100 mAs divided equally between 15 projections. The magnified mammography images were also acquired at 26 kVp using an exposure of 100 mAs. The moving-source DBT system collected these projections over an angular span of 15° and used the detector in a binned mode (pixel size: 140 μm) [21], as recommended by the manufacturer for this model. The clinical configuration of the sDBT system had been optimized in a previous study [20]. Since the

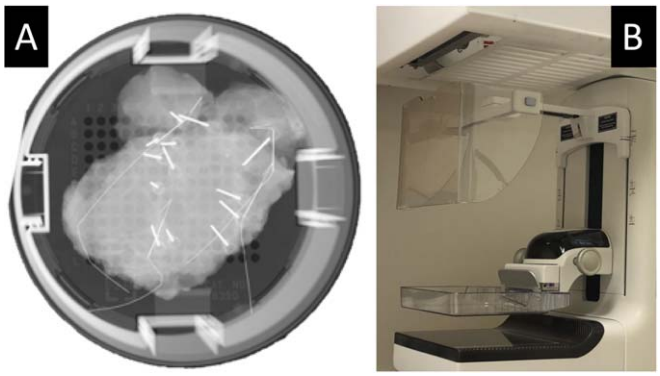

Figure 1. The lumpectomy specimens were transported and imaged in standard specimen containers. (A) A representative central projection image of a lumpectomy specimen acquired by the *stationary* digital breast tomosynthesis (sDBT) system. (B) The sDBT system is a modified Hologic Selenia Dimensions 3D mammography device in which the single x-ray source has been replaced by a fixed array of CNT-enabled sources from XinRay Systems Inc. (Morrisville, NC).

Table 1. Physical parameters of the first-generation *stationary* digital breast tomosynthesis (sDBT) device and its parent moving-source DBT system when used in their recommended configurations [20, 21]. Focal spot (FS) motion in the scan direction was calculated for the moving-source DBT system operating at 100 mAs using a previously described approach [21]. Of note, reflecting the differences in their shapes, the focal spot was modeled as a rectangle for the moving-source DBT system and as a Gaussian for sDBT, with the reported value being the full width at half maximum (FWHM). By default, sDBT uses the detector in full resolution mode. However, in this study, the projection images were also binned in post-processing to match the detector pixel size of the moving-source DBT system.

	Moving-source DBT [21]	Gen 1 sDBT [20]
Number of projection views	15	15
Angular span (degrees)	15	28
Source-to-image distance (mm)	700	700
FS dimension in scan direction (mm)	0.46	0.9 (FWHM)
FS travel distance per projection (mm)	1.65	0
Detector pixel size (mm)	0.14	0.07/0.14
Anode material	W	W
Filter material and thickness (mm)	Al (0.7)	Al (1)

stationary source array collects projections without blurring the focal spot in the scan direction, sDBT was able to achieve a wider angular span of 28° and operate the detector in full resolution mode (pixel size: 70 μm) with only a slight increase (<2 s) in the scan time relative to its binned mode. For comparison to the moving-source DBT images, the sDBT projection images were also binned during post-acquisition processing to recreate an effective detector pixel size of 140 μm, thereby equalizing this parameter of both systems. Table 1 compares the key physical parameters of the two 3D breast imaging systems used in this study.

2.3. Generating images from information in the projection views

2.3.1. Processing and reconstructing DBT images

The projection images collected from moving-source DBT and sDBT were first processed using an offset and gain nonuniformity correction, which normalized each projection prior to reconstruction [22]. The specimens contained metal localization wires and clips used to guide biopsy. Therefore, a metal artifact reduction (MAR) algorithm, similar to a previously described approach [23], was applied to each of the projection images prior to reconstruction. MAR involved segmenting metal features in the projection images by thresholding, followed by interpolation of the segmented region using the surrounding pixel values. After normalization and MAR, the projection images were reconstructed into a 3D image space with pixel sizes that replicated the 1.8× magnification introduced by the magnification stand during 2D mammography imaging [24]. The same filtered back-projection reconstruction approach (Piccolo version 4.0.5 from Real Time Tomography LCC, Villanova, PA) was applied to both sDBT and moving-source DBT, yielding reconstructed image stacks containing the same number of image slices for a given specimen. Each reconstructed slice represented a 0.5 mm incremental step in depth, and since the specimens varied significantly in thickness, the number of slices in the image stacks ranged from 12 to 65, corresponding to specimen thicknesses from 0.6 to 3.25 cm. In order to assist the readers during comparison, the reconstructed images were rotated to align the specimens with the mammography image. Figure 2 displays three representative image slices at different depths from the reconstructed image stack generated by sDBT. The reader scrolls through the image stack to identify

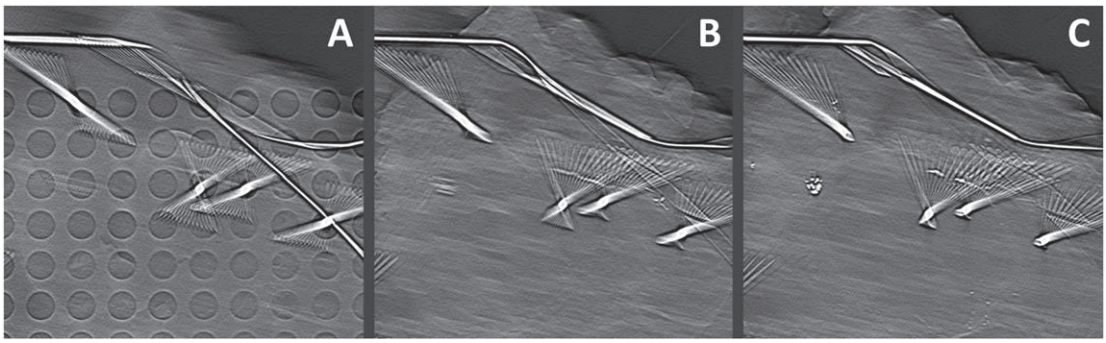

Figure 2. Image slices from a reconstructed image stack generated by *stationary* digital breast tomosynthesis (sDBT). Each slice represents a different depth measured from the x-ray detector plane: (A) 2.8 cm, (B) 3.7 cm, and (C) 4.3 cm, including the 2.5 cm gap between the detector plane and detector housing. The reader scrolls through the reconstructed image stack to identify pathology and appreciate depth relationships.

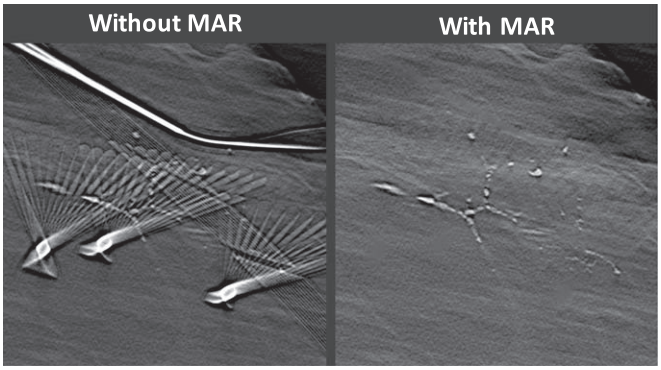

Figure 3. Representative reconstructed image slices generated by *stationary* digital breast tomosynthesis (sDBT) with and without metal artifact reduction (MAR). The application of MAR (right) removes the clutter of metal artifact that is otherwise present in the reconstructed image slices (left).

pathology and appreciate depth relationships. Figure 3 demonstrates the effects of MAR on the reconstructed image slices generated by sDBT.

2.3.2. Synthesizing the reconstructed 3D information into 2D slab images

When interpreting DBT scans, readers are now offered the option of integrating the information contained in multiple reconstructed image slices back into synthetic 2D slab images or a complete synthetic mammogram. There are many potential benefits to integrating the information in multiple reconstruction slices into a slab image, including an improved ability to appreciate microcalcification associations in clusters, since the microcalcifications are less likely to be separated in different slices through depth [25]. As such, when evaluating reader preferences during the assessment of microcalcification clusters in sDBT and moving-source DBT images, the readers were presented with slab images, created using a maximum intensity forward projection through 20 image slices (1 cm in depth) [26] in a $2 \times 2\ cm^2$ region-of-interest (ROI).

2.4. Assessing the display of individual microcalcifications and microcalcification clusters

2.4.1. Measuring microcalcification size and depth

Microcalcification size was measured as a planar area in the in-focus image slice reconstructed from both the full resolution and binned sDBT projection images and the moving-source DBT projection images (figure 4). The microcalcification sizes were reported in relation to the size of the same microcalcification measured in the magnified mammography image. Magnified 2D imaging was used as the reference for comparison, given its high spatial resolution. Individual microcalcifications were selected for study only if they were displayed by all three modalities, yielding a total of 38 individual microcalcifications in 9 of the specimens appropriate for analysis.

Area measurements were based on pixel intensities. First, a ROI was drawn manually around each microcalcification to include the adjacent background region but avoid other highly attenuating features. Segmentation of each microcalcification was accomplished by fitting Gaussian functions through the brightest pixel in both the x and y directions. The 50% intensity values of each Gaussian fit were then averaged to yield the threshold for segmentation.

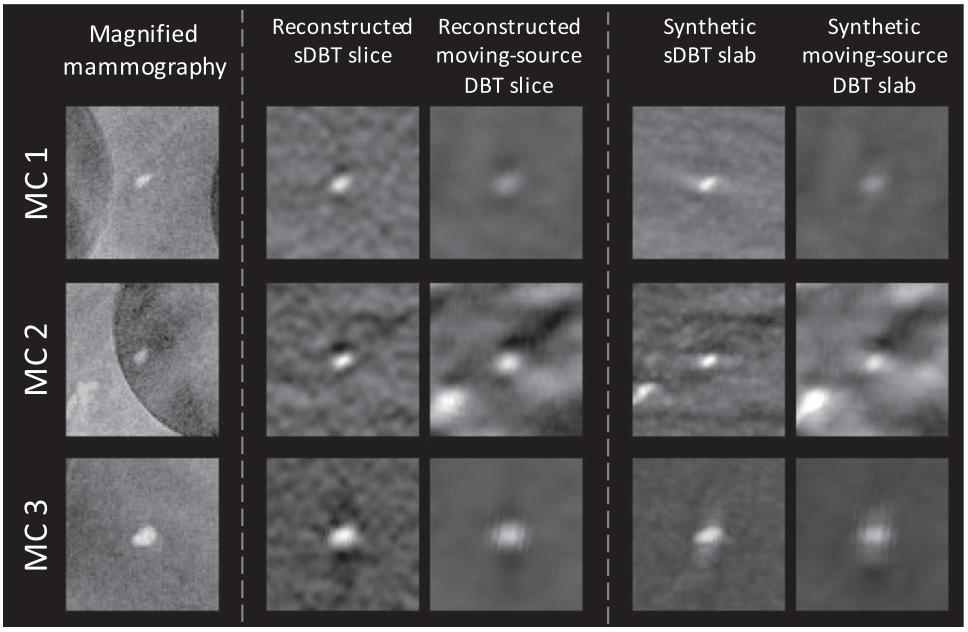

Figure 4. Example images of three microcalcifications (MC 1–3) as displayed in the magnified mammography image, the in-focus reconstructed image slices generated by *stationary* digital breast tomosynthesis (sDBT) and moving-source DBT, and the synthetic slab images generated by sDBT and moving-source DBT. Note that the microcalcifications appear less blurred in the magnified mammography images, reflecting the higher spatial resolution of this system compared to the two DBT systems. Also, note the differences in the backgrounds surrounding each microcalcification. Fewer out-of-plane features are present in the reconstructed image slices from sDBT compared to moving-source DBT, reflecting a better depth resolution as a result of the wider angular span available with the sDBT system. Mammography has no depth resolution, and thus the background includes the supporting grid. Each image represents a cropped 5 × 5 mm area at 1.8× magnification.

Segmenting all pixel values greater than this threshold provided a mask, from which the largest connected component was identified as the microcalcification. As such, the segmented region reflects the full width at half maximum (FWHM) of each microcalcification. The area was then calculated by multiplying the number of pixels in the segmented region by the area of each pixel. Since each image represents a 1.8× magnification, the pixel dimensions were divided by 1.8 when calculating the actual microcalcification size.

An artifact spread function (ASF) was used to determine the depth dimension of the microcalcification as displayed through the reconstructed image stacks of sDBT and moving-source DBT. The ASF quantifies the contrast of an attenuating feature in the reconstructed image slices above and below the in-focus plane [27]. It was calculated for each reconstructed image slice as the difference between the average intensity in the same ROI that defined the microcalcification and the average intensity of the surrounding background. Plotting the ASF as a function of distance from the in-focus plane quantifies the changing intensity with depth. Each ASF was normalized by its maximum value (from the in-focus plane). In this study, FWHM of the ASF was used as a quantitative measure to compare the depth resolution of the sDBT and moving-source DBT image stacks.

2.4.2. Assessing reader preference when viewing microcalcification clusters

The association of microcalcifications in clusters provides important diagnostic clues. As is now common in clinical practice, radiologists interpreting DBT images utilize slab images when interpreting these clusters. Slab images are generated by integrating the information from multiple slices in the reconstructed image stack into a single image, typically 1 cm in thickness (see 2.3.2 Synthesizing the reconstructed 3D information into 2D slab images). As such, when evaluating the appearance of microcalcifications in clusters in this study, readers were presented with standard 1 cm-thick slabs for viewing. Two radiologists specializing in breast imaging were asked to rate either a strong preference, preference, weak preference, or similar preference when assessing microcalcification morphology, distribution/clustering, and size using a 7-point scale (−3 to +3) when viewing pairs of images: mammography image versus sDBT slab, mammography image versus moving-source DBT slab, and sDBT slab versus moving-source DBT slab. All images were presented to the readers on MQSA-qualified 5-megapixel grayscale display monitors equipped with conventional DICOM viewing software tools. The order of individual images seen first and the order of image pairs was random. After viewing all of the image combinations for each case, the readers then ranked the three images as to their clinical usefulness,

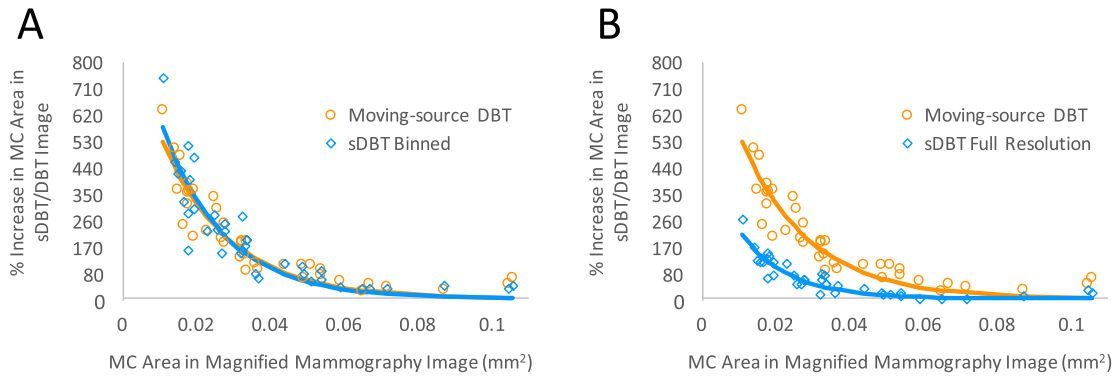

Figure 5. Comparison of the size of individual microcalcifications (MC) as displayed in the in-focus reconstructed image slice by *stationary* digital breast tomosynthesis (sDBT) (blue diamonds) and moving-source DBT (orange circles). Size refers to the planar (x-y) area of the microcalcification as seen in a single image, referenced as a percentage to the size of the same microcalcification displayed by magnified mammography. As microcalcification size decreases and begins pushing the resolution of the system, the feature is blurred. Progressive blurring produces microcalcifications that appear larger but have a lower contrast. The planar sizes of individual microcalcifications were similar in images generated by moving-source DBT and sDBT when the sDBT projections were binned by post-processing, with the binned-detector mode being the default setting for the moving-source DBT system used in these experiments (A). However, when the sDBT system was operated in its optimum configuration, including the full-resolution detector mode, the size of every microcalcification was closer to that of magnified mammography than moving-source DBT (B), suggesting that the feature was displayed with less blur.

again using a 7-point scale. The responses provided data for statistical comparison.

2.5. Statistical analysis

A one-sample t-test was used to compare the paired datasets in this study. The findings are reported as the mean and corresponding standard deviation. A p value of less than 0.05 was considered to demonstrate statistical significance.

3. Results

3.1. Measured size and depth of individual microcalcifications

The planar size of individual microcalcifications was similar in images generated by moving-source DBT and sDBT when the sDBT projections were binned by post-processing, with the binned-detector mode being the default setting for the moving-source DBT system used in these experiments (figure 5(A)). However, the unique structure of the sDBT system allowed for the collection of a wider-angle span of projection views and the operation of the detector in full-resolution mode without significantly prolonging the scan time. In this configuration, the planar sizes of individual microcalcifications displayed by sDBT were more similar to magnified mammography than moving-source DBT, a trend which was even more pronounced with decreasing microcalcification size (figure 5(B)). This trend reflects the different spatial resolutions of each system. As the microcalcification size approaches the resolution the system, it appears blurred in the image. This blurring is a progressive change of increasing relative area but decreasing contrast, as microcalcifications of smaller and smaller size are displayed. Eventually, the contrast becomes too low to distinguish the microcalcification from its background, and therefore, it cannot be detected. With this in mind, figure 5 demonstrated that sDBT, when operated in a full-resolution detector mode, displayed the smallest visible microcalcifications with less blur compared to moving-source DBT, using magnified mammography as a reference.

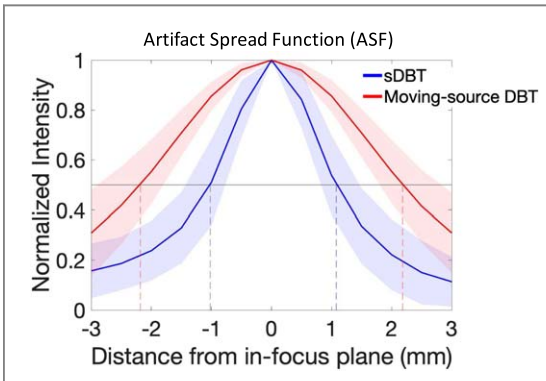

Figure 6. Comparison of the artifact spread function (ASF) of individual microcalcifications in the reconstructed image stacks generated by *stationary* digital breast tomosynthesis (sDBT) (blue) and moving-source DBT (red). ASF provides a measure of size in the depth (z) direction and thus a reflection of depth resolution. The mean ASF (solid line) is narrower with sDBT compared to moving-source DBT. This difference is statistically-significant ($p < 0.001$) when compared at the full-width half-maximum (FWHM) (dashed lines). The shaded regions represent standard deviation about the mean.

ASF is a reflection of depth resolution, and as expected, given the wider angular span of the distributed sDBT source array, for every microcalcification analyzed, sDBT yielded a narrower ASF in the reconstructed image stack compared to moving-source DBT (figure 6). This difference was statistically-significant ($p < 0.001$) when compared at the mean FWHM of the ASF for sDBT (2.1 mm) and moving-

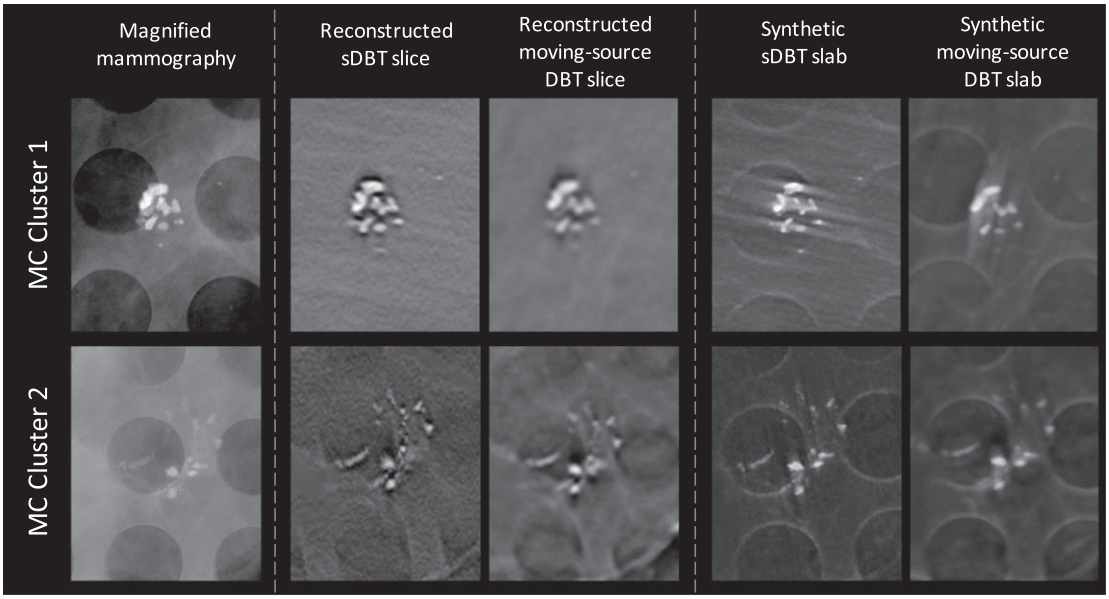

Figure 7. Example images of two microcalcification (MC) clusters as displayed in the magnified mammography image, representative slices from the reconstructed image stacks from *stationary* digital breast tomosynthesis (sDBT) and moving-source DBT, and synthetic slab images from the two DBT systems. The synthetic slab images were generated as a maximum intensity projection through 1 cm of the reconstructed image stack. However, as can be appreciated, the appearance of the microcalcifications in each cluster is similar in the reconstructed image slices and the synthetic slab image. Note that the microcalcifications appear less blurred in the magnified mammography images, reflecting the higher spatial resolution of this system compared to the two DBT systems. Each image represents a cropped 21 × 17 mm area at 1.8× magnification.

source DBT (4.4 mm). The improved ASF provided by sDBT can also be appreciated in the reconstructed image slices shown in figure 4, MC 2, as more background structures are present in the reconstructed moving-source DBT slice as a result of its smaller angular span.

3.2. Reader preference when viewing individual microcalcifications and microcalcification clusters

Synthetic slab images and complete synthetic mammograms may display the spatial association of microcalcification clusters better than the reconstructed image stack, as microcalcification distributions can be visualized in a single image. Therefore, synthetic slab images were generated for the reader preference analysis (figure 7).

Readers were asked to rate their preference when identifying small calcifications, characterizing their morphology, and assessing the distribution of clustered microcalcifications in the magnified mammography images as well as synthetic slabs generated from the image stacks reconstructed from the full resolution sDBT projections and moving-source DBT projections. Overall, readers preferred the synthetic slab image generated by sDBT and the magnified mammography image over the moving-source DBT slab image (figures 8(A) and (B)). On average, readers also tended to prefer the magnified mammography image over the sDBT slab image. However, this preference was less consistent (figure 8(C)).

In terms of characterizing the overall diagnostic value of the magnified mammography image, the sDBT synthetic slab image, and the moving-source DBT synthetic slab image, readers strongly preferred sDBT and magnified mammography over moving-source DBT ($p < 0.05$), and on average, magnified mammography was preferred over sDBT ($p < 0.05$).

4. Discussion

Microcalcification visibility was assessed in this study for several reasons. First, microcalcification morphology and distribution provide important diagnostic clues in mammography, with smaller (<0.5 mm diameter), irregularly-shaped, and numerous, tightly-clustered calcifications being of most concern for malignancy [28]. Second, debate continues regarding the adequacy of microcalcification display by 3D mammography [13, 14, 29], leading to the common practice of combining 2D and 3D mammography. Third, microcalcification visibility is a reflection of the resolution of a system, and thus, provides a clinically-applicable measure of performance by which the novel approach of *stationary* DBT can be compared to standard 2D mammography and conventional, moving-source DBT.

Despite having larger focal spot sizes, the first-generation sDBT system was able to display microcalcification sizes similar to the parent moving-source DBT system from which it was constructed, when post-processing was used to bin the sDBT images to an equal detector pixel size. This equivalence most likely reflects the absence of focal spot blurring from source

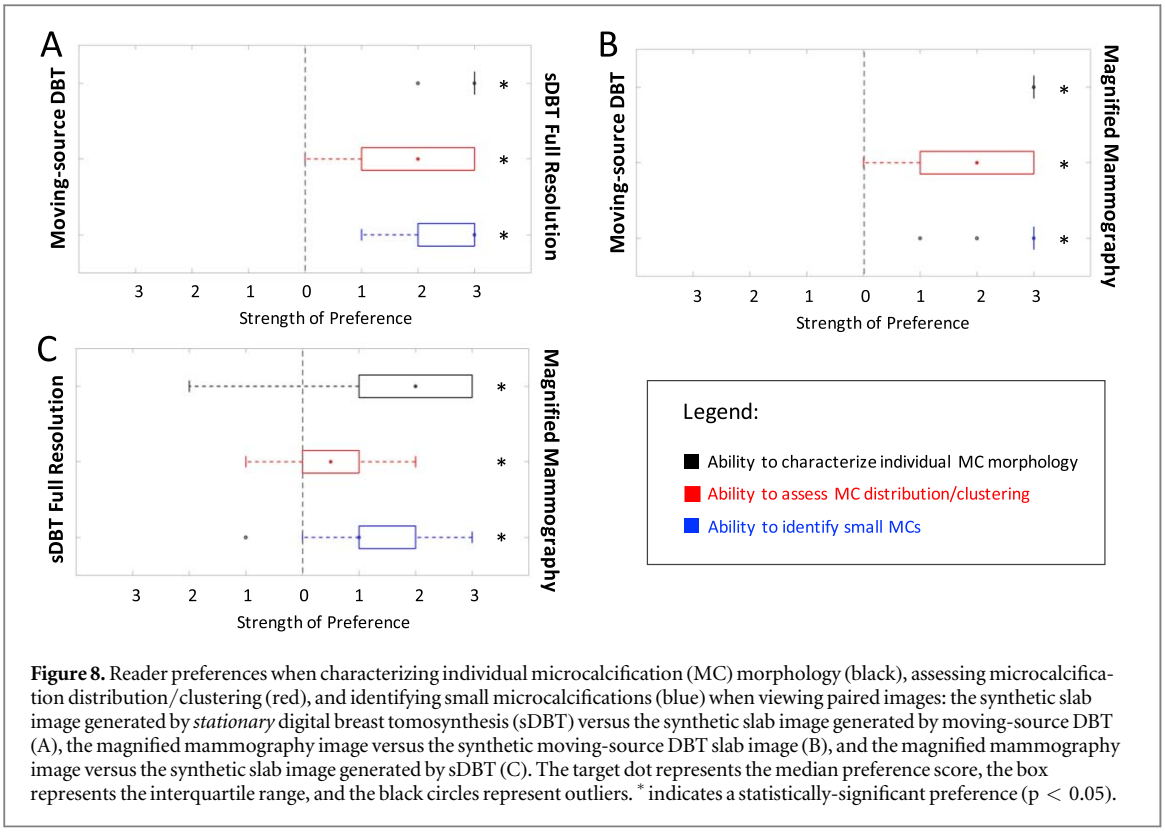

Figure 8. Reader preferences when characterizing individual microcalcification (MC) morphology (black), assessing microcalcification distribution/clustering (red), and identifying small microcalcifications (blue) when viewing paired images: the synthetic slab image generated by *stationary* digital breast tomosynthesis (sDBT) versus the synthetic slab image generated by moving-source DBT (A), the magnified mammography image versus the synthetic moving-source DBT slab image (B), and the magnified mammography image versus the synthetic slab image generated by sDBT (C). The target dot represents the median preference score, the box represents the interquartile range, and the black circles represent outliers. * indicates a statistically-significant preference ($p < 0.05$).

motion. Additionally, since sDBT is not limited by the need to move an x-ray source, a wide-angle span of projection views could be collected without significantly compromising the scan time. To demonstrate the potential benefits offered by this unique tube structure, the sDBT device was also operated with the detector in full-resolution mode while collecting projection views over a wider-angle span than the moving-source DBT system. As expected, in this configuration, sDBT displayed microcalcifications with smaller planar sizes, reflecting less blur, and narrower depth dimensions in the reconstructed image slices compared to moving-source DBT. These differences were associated with better microcalcification visibility, as reflected by reader preference when identifying small microcalcifications, characterizing the morphology of individual microcalcifications, and appreciating microcalcification distribution in synthetic slab images generated by sDBT.

Although the findings of this study are important and support the viability of this unique technology as a potential clinical tool, it should be noted that this study was not designed to compare the relative value of sDBT to moving-source DBT. First, the images were acquired at a fixed dose and therefore did not allow the systems to optimize settings, which would happen in the clinic. Second, to isolate the technical aspects of the imaging systems, reconstruction and forward projection were accomplished using the same processing steps and not the proprietary algorithms developed specifically for each device. Third, the parent moving-source DBT system to which sDBT was compared is only one of many different moving-source DBT designs, each with its own complement of hardware and software. As such, these findings must be interpreted in the broad and rapidly-evolving context of DBT in general. And finally, the findings do not define the clinical performance of sDBT, as this will require assessments of diagnostic utility across a range of soft-tissue and calcification pathologies in patients. Nevertheless, the findings are of use. Their value lies in demonstrating the potential benefits of the CNT-enabled *stationary* source array, while also pointing out directions for continued development to improve the sDBT technology.

In most cases in this study, readers preferred magnified 2D mammography over sDBT when asked to characterize microcalcifications. Indeed, as can be appreciated when comparing the magnified mammography images to images of individual microcalcifications in reconstructed image slices and microcalcification clusters in synthetic slab images, the microcalcifications appear less blurred in the magnified mammography images, reflecting the higher spatial resolution of this system. This finding is guiding ongoing research, with a goal of developing synthetic mammograms that can eliminate the need to collect a 2D mammogram at the same time as the sDBT study. Success will require improvements in both technology and image processing. For example, a second-generation sDBT device that supports a higher dose rate and wider angular span has been constructed for research [30]. Also, work continues to optimize the forward-projection algorithms that generate synthetic

2D slab images and mammograms for the unique geometry of sDBT [31].

5. Conclusion

Stationary DBT is a novel approach to 3D mammography in which the single moving x-ray source used by commercially-available DBT devices is replaced by a fixed and distributed array of separate sources made possible by CNT technology. In this study of lumpectomy specimens, the benefits of the *stationary* source array were demonstrated by assessing the visibility of microcalcifications. Additionally, the findings are also guiding continued research and development in source design and image processing, with a goal of achieving a microcalcification display with the same diagnostic value as 2D mammography.

Acknowledgments

The project was supported by the National Cancer Institute grants U54CA151652 and F30CA235892. The authors would like to thank Hologic, Inc. for technical support. Thank you to Emily Gidcumb, Jing Shan, and Marci Potuzko for support in acquiring image datasets. Otto Zhou has equity ownership and serves on the board of directors of Xintek, Inc., to which the technologies used in this project have been licensed. Jianping Lu has equity ownership in Xintek, Inc. Andrew Tucker is an employee at XinVivo, Inc. The remaining authors did not have conflicts of interest with this study. All activities have been approved by institutional conflict of interest committees.

ORCID iDs

Connor Puett https://orcid.org/0000-0001-7994-7165
Christina R Inscoe https://orcid.org/0000-0001-8681-9030
Yueh Z Lee https://orcid.org/0000-0003-1846-7680

References

[1] Siegel R L, Miller K D and Jemal A 2018 Cancer statistics, 2018 *CA: A Cancer Journal for Clinicians* **68** 7–30
[2] Monticciolo D L *et al* 2017 Breast cancer screening for average-risk women: recommendations from the ACR commission on breast imaging *Journal of the American College of Radiology* **14** 1137–43
[3] Kerlikowske K *et al* 2013 Outcomes of screening mammography by frequency, breast density, and postmenopausal hormone therapy *JAMA Intern. Med.* **173** 807–16
[4] Vedantham S, Karellas A, Vijayaraghavan G R and Kopans D B 2015 Digital breast tomosynthesis: state of the art *Radiology* **277** 663–84
[5] Lei J, Yang P, Zhang L, Wang Y and Yang K 2014 Diagnostic accuracy of digital breast tomosynthesis versus digital mammography for benign and malignant lesions in breasts: a meta-analysis *Eur. Radiol.* **24** 595–602
[6] Helvie M A 2010 Digital mammography imaging: breast tomosynthesis and advanced applications *Radiologic Clinics of North America* **48** 917–29
[7] Hooley R J, Durand M A and Philpotts L E 2016 Advances in digital breast tomosynthesis *American Journal of Roentgenology* **208** 256–66
[8] Skaane P *et al* 2013 Comparison of digital mammography alone and digital mammography plus tomosynthesis in a population-based screening program *Radiology* **267** 47–56
[9] Durand M A *et al* 2014 Early clinical experience with digital breast tomosynthesis for screening mammography *Radiology* **274** 85–92
[10] Lourenco A P, Barry-Brooks M, Baird G L, Tuttle A and Mainiero M B 2014 Changes in recall type and patient treatment following implementation of screening digital breast tomosynthesis *Radiology* **274** 337–42
[11] Rose S L, Tidwell A L, Bujnoch L J, Kushwaha A C, Nordmann A S and Sexton R 2013 Implementation of breast tomosynthesis in a routine screening practice: an observational study *Am. J. of Roentgenology* **200** 1401–8
[12] McCarthy A M *et al* 2014 Screening outcomes following implementation of digital breast tomosynthesis in a general-population screening program *J Natl. Cancer Inst* **106** (11) dju316
[13] Spangler M L *et al* 2011 Detection and classification of calcifications on digital breast tomosynthesis and 2D digital mammography: a comparison *AJR Am. J Roentgenol* **196** 320–4
[14] Tagliafico A *et al* 2014 Characterisation of microcalcification clusters on 2D digital mammography (FFDM) and digital breast tomosynthesis (DBT): does DBT underestimate microcalcification clusters? Results of a multicentre study *Eur Radiol.* **25** 9–14
[15] Sickles E A, D'Orsi C J and Bassett L W 2013 *ACR BI-RADS® Mammography. In: ACR BI-RADS® Atlas, Breast Imaging Reporting and Data System* (Reston, VA: American College of Radiology)
[16] Gao Y, Babb J S, Toth H K, Moy L and Heller S L 2017 Digital breast tomosynthesis practice patterns following 2011 FDA approval: a survey of breast imaging radiologists *Acad Radiol.* **24** 947–53
[17] US Food and Drug Administration 2013 Selenia Dimensions Digital Breast Tomosynthesis Premarket Approval (PMA) Published May 23, 2013. Accessed July 22, 2019. https://accessdata.fda.gov/scripts/cdrh/cfdocs/cfpma/pma.cfm?id=P080003S001
[18] US Food and Drug Administration 2017 Senoclaire Digital Breast Tomosynthesis Premarket Approval (PMA). Published January 5, 2017. Accessed July 22, 2019. https://accessdata.fda.gov/scripts/cdrh/cfdocs/cfPMA/pma.cfm?id=P130020S001
[19] Qian X *et al* 2012 High resolution *stationary* digital breast tomosynthesis using distributed carbon nanotube x-ray source array *Med. Phys.* **39** 2090–9
[20] Tucker A W, Lu J and Zhou O 2013 Dependency of image quality on system configuration parameters in a *stationary* digital breast tomosynthesis system *Med. Phys.* **40** 031917
[21] Marshall N W and Bosmans H 2012 Measurements of system sharpness for two digital breast tomosynthesis systems *Phys. Med. Biol.* **57** 7629
[22] Puett C, Inscoe C, Lee Y Z, Zhou O and Lu J 2018 Phantom-based study exploring the effects of different scatter correction approaches on the reconstructed images generated by contrast-enhanced *stationary* digital breast tomosynthesis *JMI, JMIOBU* **5** 013502
[23] Puett C *et al* 2018 *Stationary* digital intraoral tomosynthesis: demonstrating the clinical potential of the first-generation system *Medical Imaging 2018: Physics of Medical Imaging* 105730E (10573) *(Houston, TX, March 2018)*

[24] Tucker A W *et al* 2014 Comparison of a *stationary* digital breast tomosynthesis system to magnified 2D mammography using breast tissue specimens *Academic Radiology.* **21** 1547–52
[25] Zuley M L *et al* 2014 Comparison of two-dimensional synthesized mammograms versus original digital mammograms alone and in combination with tomosynthesis images *Radiology* **271** 664–71
[26] Diekmann F *et al* 2009 Thick slices from tomosynthesis data sets: phantom study for the evaluation of different algorithms *J Digit Imaging* **22** 519–26
[27] Wu T, Moore R H, Rafferty E A and Kopans D B 2004 A comparison of reconstruction algorithms for breast tomosynthesis *Med. Phys.* **31** 2636–47
[28] Henrot P, Leroux A, Barlier C and Génin P 2014 Breast microcalcifications: the lesions in anatomical pathology *Diagnostic and Interventional Imaging* **95** 141–52
[29] Kopans D, Gavenonis S, Halpern E and Moore R 2011 Calcifications in the breast and digital breast tomosynthesis *Breast J.* **17** 638–44
[30] Calliste J *et al* 2017 Second generation *stationary* digital breast tomosynthesis system with faster scan time and wider angular span *Med. Phys.* **44** 4482–95
[31] Puett C, Inscoe C, Lu J, Lee Y and Zhou O 2019 Generating synthetic mammograms for *stationary* 3D mammography *Medical Imaging 2019: Physics of Medical Imaging* 1094807 (10948) *(San Diego, CA, March 2019)*